

Elastic softness of hybrid lead halide perovskites

A.C. Ferreira,^{1,2} A. Létoublon,² S. Paofai,³ S. Raymond,⁴ C. Ecolivet,⁵ B. Rufflé,⁶ S. Cordier,³ C. Katan,³ M. I. Saidaminov,⁷ A. A. Zhumekenov,⁷ O. M. Bakr,⁷ J. Even,² and P. Bourges¹

¹Laboratoire Léon Brillouin, CEA-CNRS, Université Paris-Saclay, CEA Saclay, 91191 Gif-sur-Yvette, France

²Laboratoire FOTON, INSA, Université Rennes, F-35708 Rennes France

³Institut des Sciences Chimiques de Rennes, CNRS, Université de Rennes 1, Ecole Nationale Supérieure de Chimie de Rennes, INSA de Rennes, 35042 Rennes, France

⁴Univ. Grenoble Alpes, CEA, INAC, MEM, 38000 Grenoble, France

⁵Univ Rennes, CNRS, IPR [(Institut de Physique de Rennes)] UMR 6251, F-35000 Rennes, France

⁶Laboratoire Charles Coulomb (L2C), UMR 5221 CNRS-Université de Montpellier, Montpellier, FR-34095, France

⁷King Abdullah University of Science and Technology (KAUST), KAUST Catalysis Center, KAUST Solar Center,

Physical Sciences and Engineering Division (PSE), Thuwal 23955-6900, Saudi Arabia

(Dated: January 29, 2018)

Much recent attention has been devoted towards unravelling the microscopic optoelectronic properties of hybrid organic-inorganic perovskites (HOP). Here we investigate by coherent inelastic neutron scattering spectroscopy and Brillouin light scattering, low frequency acoustic phonons in four different hybrid perovskite single crystals: MAPbBr₃, FAPbBr₃, MAPbI₃ and α -FAPbI₃ (MA: methylammonium, FA: formamidinium). We report a complete set of elastic constants characterized by a very soft shear modulus C_{44} . Further, a tendency towards an incipient ferroelastic transition is observed in FAPbBr₃. We observe a systematic lower sound group velocity in the technologically important iodide-based compounds compared to the bromide-based ones. The findings suggest that low thermal conductivity and hot phonon bottleneck phenomena are expected to be enhanced by low elastic stiffness, particularly in the case of the ultrasoft α -FAPbI₃.

Motivated by environmental and energy issues, hybrid organolead perovskites (HOP) have drawn a lot of interest in the field of photovoltaic cells [1–7]. Currently, the state-of-the-art of HOP solar cells is based on alloys where methylammonium (MA) and formamidinium (FA) are both present in the same structure and *ca.* 10% are replaced by rubidium (Rb) and caesium (Cs) atoms, together with concomitant alloying of iodide (I)/bromide (Br) halogens [8], now reaching power conversion efficiencies (PCEs) in excess of 22% [9]. The rapid emergence and success of hybrid perovskites is widely attributed to various features such as low cost and low temperature processing, suitable optical bandgap (especially for iodide based HOPs), superb optical absorption across the visible spectrum, low exciton binding energies and long charge-carrier diffusion lengths. Much recent attention has been devoted towards HOPs charge-carrier features [10–13] and previous experimental studies have successfully evidenced the influence of crystal structure on their optoelectronic properties, as exemplified with the effect of octahedral tilt on the band-gap [14, 15]. However, the origin of the softness of HOPs, compared to classic semiconductors, and its influence on their charge-carrier dynamics is still lacking a comprehensive understanding and systematic experimental studies. Furthermore, in perovskite based thin film solar cells, device performance is deeply affected by film quality and fabrication processing (morphological effects, grain boundaries, etc.), which makes it difficult to study the intrinsic properties of HOPs. Single crystals, on the other hand, provide the ideal platform to uncover their fundamental limits.

In this work, we have investigated low frequency structural excitations in the cubic phases of the most relevant compounds implemented in HOPs, namely MAPbBr₃, FAPbBr₃, MAPbI₃ and α -FAPbI₃, in their single crystal form. For additional information regarding structure and crystal growth please refer to the Supplemental Material [16]. We report a complete set of elastic constants, via the corresponding sound velocities, and we relate the results to the lower thermal conductivity found in HOP compounds and the hot phonon bottleneck hypothesis proposed for such systems. For that purpose, dispersions of the acoustic phonons have been measured around main Bragg reflections using inelastic neutron scattering (INS). Complementary Brillouin light scattering (BLS) experiments have also been used to determine sound velocities in the bromide-based compounds. The experimental conditions and procedure of both techniques are detailed in the Supplemental Material [16].

Fig. 1 shows the low energy INS spectra of transverse acoustic (TA) phonons in MAPbBr₃, FAPbBr₃, MAPbI₃ and α -FAPbI₃, measured around the Bragg reflection (200). Additional data around other Bragg reflections, (110) and (111), can be found in the Supplemental Material [16]. We performed both constant energy and Q scans at the main Bragg positions. Using the (200) position as an example, longitudinal (LA) and transverse (TA) acoustic modes were measured at different reciprocal space positions $Q = (200) + q$ in HKL units, with q along (LA) and perpendicular (TA) to [200] (for TA q is parallel to [011]). Clear acoustic phonon modes are observed on top of a background. As shown by constant Q-

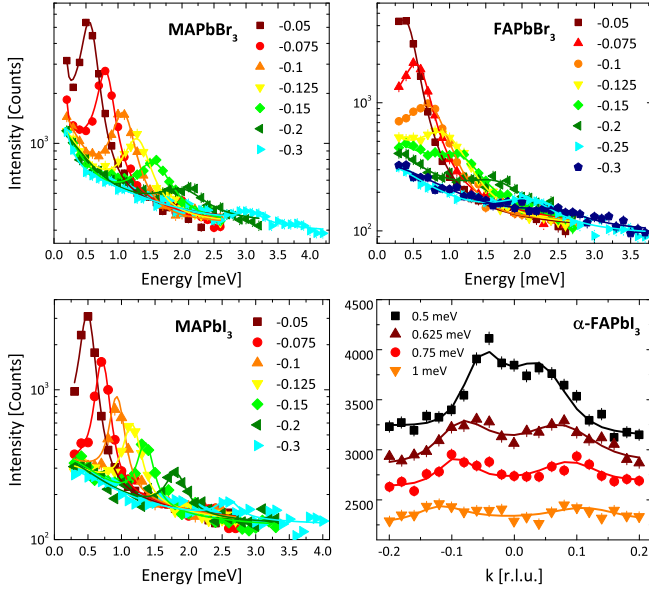


FIG. 1. Transverse acoustic (TA) phonon spectra measured by inelastic neutron scattering in the cubic phase of (a) MAPbBr₃, (b) FAPbBr₃, (c) MAPbI₃ and (d) α -FAPbI₃, for different Q positions going away from the (002) \equiv (200) Bragg peak (*i.e.* $Q = (k \ k \ 2)$) and for different energy values. With the exception of MAPbI₃ (340 K), all other compounds were studied at room temperature (RT).

scans, the background results from large quasi-elastic signals, likely coming from incoherent scattering of hydrogen atom excitations present in the MA/FA molecules, as it has been previously studied on powder samples in MAPbBr₃ [17]. Energy scans performed at various momentum vectors around the Bragg positions revealed that the quasi-elastic signal occurring in the energy window of the acoustic phonons is almost independent of the sample orientation and weakly dependent of the longitudinal momentum. The quasi-elastic signal corresponds to a flat contribution in constant-energy scans, whereas acoustic phonons show up as a double peak structure at symmetric positions of the Bragg reflection (*e.g.* Fig. 1(d)). As a result, even though the background is relatively large, one can easily separate it from the dispersing and symmetric phonon modes. All neutron spectra have been fitted as described in the Supplemental Material [16], from which the phonon energy can be extracted.

By varying the distance q to the nearest Bragg peak, Γ point, one can draw the dispersion curves, which are reported in Fig. 2 and in Supplemental Material [16]. Each sub-figure represents measurements at a different Bragg position or propagation direction. We derive the phonon sound velocity V from linear regressions along most directions and then, with simple rules of elasticity in cubic systems [18], readily determine the corresponding elastic constants for the four perovskite compounds. Fig. 2(a) and 2(b) specifically show the sound ve-

locities of transverse and longitudinal acoustic phonons around the (002) Bragg reflection. These respectively yield C_{44} and C_{11} in a rather direct way ($C = \rho V^2$) which are then plotted as a function of the lattice constant in Fig. 2(c). A summary of the determined sound velocities by INS for all four HOP compounds is given in the Supplemental Material [16] and the extracted elastic constants are in Table 1. Considering the obtained elastic constants we can also calculate the bulk modulus $K = 1/3(C_{11} + 2C_{12})$ [18], Zener anisotropy index $A = 2C_{44}/(C_{11} - C_{12})$ [19] and longitudinal/transverse (L/T) ratio for all systems (see Supplemental Material [16]).

Immediately we note that C_{12} in α -FAPbI₃ is negative, but still it respects the necessary Born elastic stability criteria for cubic systems [20, 21]. A negative C_{12} simply implies that a cubic material, when uniaxially compressed along a [100] direction, will contract in the other two directions ([010] and [001]) and in that way, try to maintain an isotropic structure. Nonetheless, the negative C_{12} together with the very low bulk modulus, confirms the very unstable nature of α -FAPbI₃ (whose metastable single crystals last less than a week in the α phase [22]) and why it has actually been paired with MA, Rb and Cs for better performing photovoltaic devices. As shown in Table 1, the four perovskite compounds exhibit an overall sizeable elastic anisotropic nature ($A \neq 1$), which can be mostly attributed to the very low shear modulus C_{44} . MAPbI₃ stands out with its relatively higher (around double) C_{44} which results in a discrepant, although still anisotropic, Zener index. However, it should be noted that the measurements were performed at 340 K, just above the transition to the cubic phase [23], resulting in an additional anharmonicity effect. The remarkably low shear moduli are much more evident when compared to the ones of classical semiconducting materials such as GaAs, AlAs, etc., where the elastic constants are in the 10^2 GPa order [24]. It is believed that the rotation/tilts of the corner sharing PbX₆ octahedra [25] could be responsible for the particularly low shear modulus and large anisotropy in HOPs.

As evidenced in Fig. 2(c), C_{11} and K decrease noticeably with increasing lattice constant. These two quantities are, therefore, lower in iodide-based systems compared with bromide ones, especially in α -FAPbI₃ where they are a third of its bromide counterpart. This indicates a structural instability when the lattice parameter exceeds 6.4 Å. The relatively higher bulk modulus in MA-based compounds should be related to a steric effect, where the more symmetric and rotating MA molecules lead to more compact structures, which in turn results in larger binding elastic interactions. It is worth emphasizing that, by construction, the acoustic branches are defining the lowest zone boundary phonons and thus, related to the lowest peaks of the phonon density of states. That also implies that the Debye temperature is very small

TABLE I. Summary of the elastic properties at RT for MAPbBr₃, FAPbBr₃, and α -FAPbI₃ and at 340 K for MAPbI₃, as measured by Inelastic Neutron Scattering (INS) and Brillouin Scattering (BS). In α -FAPbI₃, the bulk modulus is found: $K = 0.1 \pm 2.3$ GPa (we here only quote the positive range which is only physically meaningful).

Elastic Constant	MAPbBr ₃		FAPbBr ₃		MAPbI ₃		FAPbI ₃	
	INS	BS	INS	BS	INS	BS	INS	BS
C₁₁ [GPa]	34.5 \pm 1.2	32.2 \pm 0.2	27.7 \pm 1.6	31.2 \pm 0.2	21.8 \pm 1.3	n/a	11.1 \pm 2.0	n/a
C₄₄ [GPa]	4.1 \pm 0.2	3.4 \pm 0.1	3.1 \pm 0.1	1.5 \pm 0.1	7.3 \pm 0.3	n/a	2.7 \pm 0.3	n/a
C₁₂ [GPa]	18.5 \pm 2.0	9.1 \pm 0.8	11.5 \pm 2.4	9.4 \pm 0.5	11.3 \pm 3.1	n/a	-5.5 \pm 2.2	n/a
Bulk modulus [GPa]	23.9 \pm 1.3	16.8 \pm 0.1	16.9 \pm 1.7	16.667 \pm 0.3	14.8 \pm 1.7	n/a	0.0-2.4	n/a
Anisotropy, A	0.52 \pm 0.005	0.29 \pm 0.01	0.38 \pm 0.03	0.14 \pm 0.01	1.38 \pm 0.22	n/a	0.4 \pm 0.2	n/a
L/T ratio	8.7 \pm 0.5	9.5 \pm 0.3	8.9 \pm 0.7	20.8 \pm 1.4	3.0 \pm 0.2	n/a	4.3 \pm 0.9	n/a

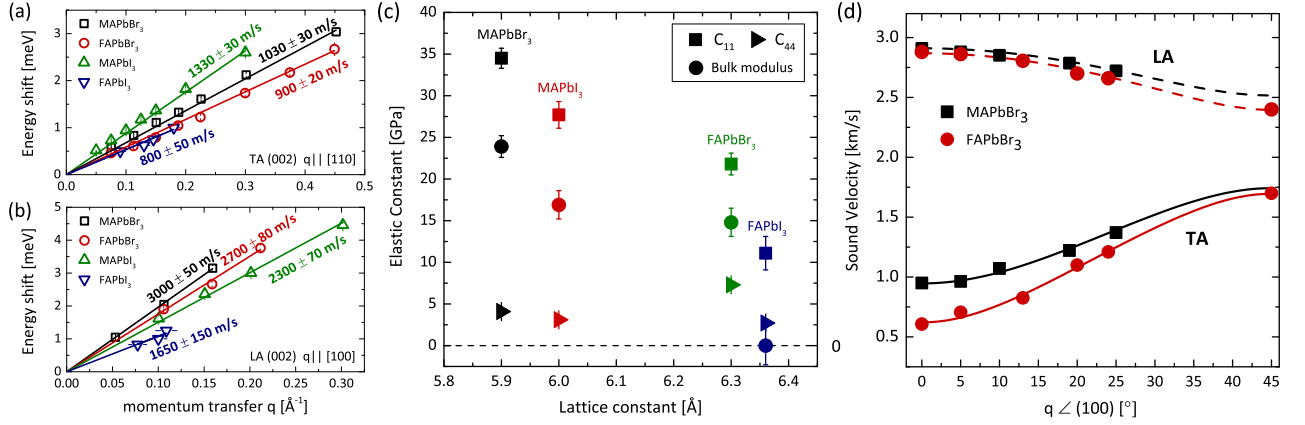


FIG. 2. Acoustic phonon dispersion curves of the four HOP (a) TA and (b) LA phonons close to the (002) Bragg reflection, measured by INS. The data for a given configuration (q direction) is regrouped for the different HOP systems and differentiated by different colors and symbols. (c) Elastic constants C_{11} and C_{44} (black) as well as the bulk modulus K (red) behaviour as a function of the changing lattice constant between compounds. (d) Sound velocity diagram for FAPbBr₃ and MAPbBr₃, as determined by Brillouin light scattering. The velocity is given as a function of the angle between the direction of measurement and the [100] direction.

(*i.e.* about 30 K). More, as a function of lattice constant, this quantity exhibits the same trend as for C_{11} and the bulk modulus. The observation that iodide materials are softer than bromide materials, as well as FA-based compounds versus MA-based ones is consistent with recent static nanoindentation measurements of the Young modulus [26, 27], though α -FAPbI₃ was not explored (see table in Supplemental Material [16] for comparison). In contrast, recent pulse-echo ultrasonic measurements at low frequency (10 MHz) and in the 140-350 K temperature range [28], show larger sound velocities for MAPbI₃ than for MAPbBr₃. However, the results of Anusca *et al.* [28] are also in disagreement with other ultrasonic studies [29, 30]. Yet it should be noted that the sound velocity attenuation is very large at 10 MHz and strongly affected by the structural phase transitions. Brillouin light scattering on the other hand, allows exploring the same properties in the GHz range, intermediate between ultrasonic and neutron scattering measurements.

Sound velocities were measured in both bromides compounds at room temperature (RT) using Brillouin light

scattering, with a set-up in the [100], [010] base plane [29]. Five different incidence angles between the normal (0°) and the Brewster angle (25°) are reported in **Fig. 3(a)** with the observation of quasi longitudinal and quasi transverse acoustic modes. A measurement along the cubic diagonal [110] is also shown. For both bromide compounds, a good agreement between INS and BLS longitudinal sound velocities is observed (see Supplemental Material [16]). The same applies for the transverse mode in MAPbBr₃ [29], within a 5% difference. In contrast, a 30% difference is observed for the same mode in FAPbBr₃. This is emphasized in **Fig. 3(b)** where the sound velocity is presented as a function of q . One can clearly observe the phonon softening of the transverse mode at lower q , in the BLS regime, which indicates a tendency towards a ferroelastic phase transition [31]. Recording that this specific sound velocity is related to the C_{44} elastic constant as $C_{44} = \rho V^2$ (where $\rho = 4087$ kg/cm³ is the density of FAPbBr₃), it means that a 30% softening of the sound velocity corresponds to a 60% re-normalization of C_{44} . Interestingly, the values

obtained by laser ultrasonics [30], where a set of elastic constants was also given for MAPbBr₃, are in good agreement with our BLS results and a similar softening of C_{44} is observed too.

The softening of the C_{44} elastic constant is typically related to the proximity of a ferroelastic transition [31] which, in this case, can be only incipient. To test that possibility, we have performed a temperature study of the acoustic branch using INS. A softening of acoustic phonon at $\mathbf{Q} = (2, 0.025, 0.025)$ is indeed observed right below RT in FAPbBr₃. As shown in **Fig. 3(b)**, the shear modulus C_{44} is drastically reduced upon cooling, however, that effect is stabilized below ~ 270 K. Actually, this temperature range corresponds to the growing of an additional scattering in elastic neutron scattering at the M point, like *e.g.* $\mathbf{Q} = (3/2, 1/2, 0)$ (**Fig. 3(b)**). The measurements of the M point intensity show the appearance of a phase transition at 263 K in FAPbBr₃ towards a tetragonal structure, characterized by a doubling of the cubic unit cell. In general, lead perovskites are indeed known to exhibit structural instabilities at both the M and R points [32]. From **Fig. 3.b**, one can see that the phase transition is blocking the development of the ferroelastic instability, limiting pre-translational effects at high temperature, compared to what would be expected for a true ferroelastic transition [31]. By linearly extrapolating the high temperature behaviour, we can estimate that such a ferroelastic transition would occur at 240 ± 20 K, barring the occurrence of the structural instability at the M point. Consistently with an aborted ferroelastic instability, a very modest phonon broadening is observed with decreasing temperature from 300 to 230 K.

HOPs are characterized by high electron/hole free charge carrier mobility at room temperature. At high temperature ranges such as RT (10 times the Debye temperature), the electronic mobility, μ , is typically governed by phonon scattering, via electron-phonon coupling (Fröhlich phonon emission). The whole phonon spectrum will then contribute to the electronic scattering rate, $1/\tau$ (μ is proportional to the electronic relaxation time τ). However, for intra-valley electron bands of direct gap semiconductors like the 3D HOP, the scattering rate should also be enhanced by collisions with low energy longitudinal acoustic phonons. When the acoustic phonon contribution is considered, the electronic scattering time, τ , is expected to be proportionnal to the average squared longitudinal sound velocities [33], *i.e.* proportional to the average elastic constants such as C_{11} or the bulk modulus K that are shown in **Fig. 2(c)**. The contributions to the carrier mobilities related to interactions with acoustic phonons are thus predicted to be strongly different between iodide- and bromide-based compounds, but such a large difference is not experimentally observed here. Instead, it further shows that the carrier mobilities are rather limited by other processes, namely interactions with optical phonons. Such observa-

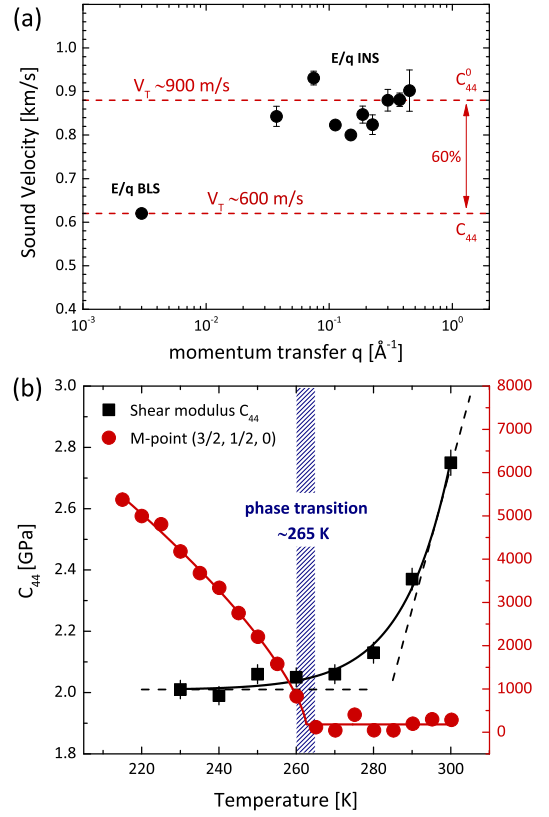


FIG. 3. Softening of C_{44} in FAPbBr₃ (a) as function of q (at RT) and (b) as a function of temperature (230 - 300 K), around the (002) Bragg reflection. Also in (b) the Bragg M point intensity (red) across a similar temperature range. The bare elastic constant, C_{44}^0 , represents the elastic properties without the influence of the (incipient) phase transition. Note that the q scale is logarithmic to underline the broad q -range covered by both experimental techniques.

tion is corroborated by emission line broadening results [34, 35], and it confirms that scattering from longitudinal optical phonons is the dominant source of electron-phonon coupling near RT.

It is necessary, however, to consider the acoustic phonons in order to explain other optoelectronic properties that Fröhlich optical phonon emission does not account for. More precisely, a significant hot-phonon bottleneck effect in carrier thermalization is observed in lead-halide perovskites [36, 37], when carrier injection levels are high. This is explained by the up-conversion of acoustic phonons which recycle thermal (vibrational) energy, reheating charge carriers and prolonging the cooling period of carrier-optical phonon system. Ultrafast transient absorption measurements reveal two stages of the carrier cooling process [37]. The first one is related to the intrinsic Fröhlich phonon emission mentioned above and does not vary significantly among the various different perovskites. On the other hand, in the second cooling stage, hot carrier-phonon dynamics occur, corresponding

to a phonon bottleneck effect [36, 37]. The various HOP materials studied in the present work show, in fact, very different acoustic phonon densities of states that might affect hot phonon energy relaxations. At RT, the carrier-phonon relaxation rate of that second cooling stage is typically 3 times slower in α -FAPbI₃, compared with the MAPbBr₃ system [37]. This is fully consistent with the difference in elastic constants reported in **Fig. 2(c)**.

Another direct consequence of the lattice softness is the ultralow thermal conductivities reported in perovskites [38]. Thermal conductivity is typically proportional to the square of the phonon sound group velocity [33, 38], corresponding to an average elastic constant (**Fig. 2(c)**). One can then associate lower thermal conductivity to lower elastic stiffness [27, 39, 40]. It is worth mentioning that a strong phonon bottleneck effect is essential for hot carrier photovoltaic devices, as it allows for a long-lived hot carrier population. Lower elastic bulk modulus, sign of low thermal conductivity, appears to be, therefore, important to enhance the hot carrier effect.

In conclusion, our quantitative study of low energy acoustic phonons presents a complete set of elastic constants of various technologically relevant hybrid perovskites, in their cubic phases, and shows a noticeable variation of elastic bulk modulus among them. We give a clear explanation for the ultralow thermal conductivities measured in hybrid organolead perovskites. Moreover, the data presented here strongly supports the hypothesis of the hot phonon bottleneck phenomena, reported by other authors to explain hot carriers relaxations. Both processes are expected to be enhanced by low elastic stiffness, especially in the case of the ultrasoft α -FAPbI₃.

-
- [1] A. Kojima, K. Teshima, Y. Shirai, and T. Miyasaka, *Journal of the American Chemical Society* **131**, 6050 (2009).
 - [2] D. B. Mitzi, C. D. Dimitrakopoulos, and L. L. Kosbar, *Chemistry of materials* **13**, 3728 (2001).
 - [3] J. L. Knutson, J. D. Martin, and D. B. Mitzi, *Inorganic chemistry* **44**, 4699 (2005).
 - [4] N.-G. Park, *Materials Today* **18**, 65 (2015).
 - [5] W. S. Yang, J. H. Noh, N. J. Jeon, Y. C. Kim, S. Ryu, J. Seo, and S. I. Seok, *Science* **348**, 1234 (2015).
 - [6] E. H. Anaraki, A. Kermanpur, L. Steier, K. Domanski, T. Matsui, W. Tress, M. Saliba, A. Abate, M. Grätzel, A. Hagfeldt, *et al.*, *Energy & Environmental Science* **9**, 3128 (2016).
 - [7] "NREL chart," http://www.nrel.gov/pv/assets/images/efficiency_chart.php, accessed: 25.03.2017.
 - [8] M. Saliba, T. Matsui, K. Domanski, J.-Y. Seo, A. Ummadisingu, S. M. Zakeeruddin, J.-P. Correa-Baena, W. R. Tress, A. Abate, A. Hagfeldt, *et al.*, *Science* **354**, 206 (2016).
 - [9] W. S. Yang, B.-W. Park, E. H. Jung, N. J. Jeon, Y. C. Kim, D. U. Lee, S. S. Shin, J. Seo, E. K. Kim, J. H. Noh, *et al.*, *Science* **356**, 1376 (2017).
 - [10] Y. Yamada, T. Nakamura, M. Endo, A. Wakamiya, and Y. Kanemitsu, *Journal of the American Chemical Society* **136**, 11610 (2014).
 - [11] V. D'Innocenzo, G. Grancini, M. J. Alcocer, A. R. S. Kandada, S. D. Stranks, M. M. Lee, G. Lanzani, H. J. Snaith, and A. Petrozza, *Nature communications* **5**, 3586 (2014).
 - [12] C. Wehrenfennig, G. E. Eperon, M. B. Johnston, H. J. Snaith, and L. M. Herz, *Advanced materials* **26**, 1584 (2014).
 - [13] L. M. Herz, *Annual review of physical chemistry* **67**, 65 (2016).
 - [14] J. Even, L. Pedesseau, J.-M. Jancu, and C. Katan, *The Journal of Physical Chemistry Letters* **4**, 2999 (2013).
 - [15] J. Even, L. Pedesseau, and C. Katan, *The Journal of Physical Chemistry C* **118**, 11566 (2014).
 - [16] *see Supplemental Material* <http://link.aps.org/supplemental/...> for supporting information.
 - [17] I. P. Swainson, C. Stock, S. F. Parker, L. Van Eijck, M. Russina, and J. W. Taylor, *Physical Review B* **92**, 100303(R) (2015).
 - [18] D. Halliday, R. Resnick, and J. Walker, *Fundamentals of Physics. 5th Extended* (Wiley, 1997).
 - [19] C. Zener, *Elasticity and anelasticity of metals* (University of Chicago, 1948).
 - [20] M. Born, in *Mathematical Proceedings of the Cambridge Philosophical Society*, Vol. 36 (Cambridge Univ Press, 1940) pp. 160–172.
 - [21] F. Mouhat and F.-X. Coudert, *Physical Review B* **90**, 224104 (2014).
 - [22] A. A. Zhumekenov, M. I. Saidaminov, M. A. Haque, E. Alarousu, S. P. Sarmah, B. Murali, I. Dursun, X.-H. Miao, A. L. Abdelhady, T. Wu, *et al.*, *ACS Energy Letters* **1**, 32 (2016).
 - [23] P. Whitfield, N. Herron, W. Guise, K. Page, Y. Cheng, I. Milas, and M. Crawford, *Scientific reports* **6**, 35685 (2016).
 - [24] I. Vurgaftman, J. Meyer, and L. Ram-Mohan, *Journal of applied physics* **89**, 5815 (2001).
 - [25] I. Swainson, M. Tucker, D. Wilson, B. Winkler, and V. Milman, *Chemistry of materials* **19**, 2401 (2007).
 - [26] Y. Rakita, S. R. Cohen, N. K. Kedem, G. Hodes, and D. Cahen, *MRS Communications* **5**, 623 (2015).
 - [27] G. A. Elbaz, W.-L. Ong, E. A. Doud, P. Kim, D. W. Paley, X. Roy, and J. A. Malen, *Nano Letters* (2017).
 - [28] I. Anusca, S. Balčiūnas, P. Gemeiner, Š. Svirskas, M. Sanlialp, G. Lackner, C. Fettkenhauer, J. Belovickis, V. Samulionis, M. Ivanov, *et al.*, *Advanced Energy Materials* (2017).
 - [29] A. Létoublon, S. Paofai, B. Rufflé, P. Bourges, B. Hehlen, T. Michel, C. Ecolivet, O. Durand, S. Cordier, C. Katan, *et al.*, *The Journal of Physical Chemistry Letters* **7**, 3776 (2016).
 - [30] A. M. Lomonosov, X. Yan, C. Sheng, V. E. Gusev, C. Ni, *Journal of Applied Physics* **117**, 115501 (2015).
 - [31] H. Cummins, *Phil. Trans. R. Soc. Lond. A* **293**, 393 (1979).
 - [32] Y. Fujii, S. Hoshino, Y. Yamada, and G. Shirane, *Physical Review B* **9**, 4549 (1974).
 - [33] R. G. Chambers, *Electron in Metals and Semiconductors*, (1990).
 - [34] A. D. Wright, C. Verdi, R. L. Milot, G. E. Eperon, M. A.

- Pérez-Osorio, H. J. Snaith, F. Giustino, M. B. Johnston, and L. M. Herz, *Nature communications* **7** (2016).
- [35] H. Diab, G. Trippé-Allard, F. Lédée, K. Jemli, C. Vilar, G. Bouchez, V. L. Jacques, A. Tejeda, J. Even, J.-S. Lauret, *et al.*, *The journal of physical chemistry letters* **7**, 5093 (2016).
 - [36] Y. Yang, D. P. Ostrowski, R. M. France, K. Zhu, J. Van De Lagemaat, J. M. Luther, and M. C. Beard, *Nature Photonics* **10**, 53 (2016).
 - [37] J. Yang, X. Wen, H. Xia, R. Sheng, Q. Ma, J. Kim, P. Tapping, T. Harada, T. W. Kee, F. Huang, *et al.*, *Nature Communications* **8** (2017).
 - [38] M. Wang and S. Lin, *Adv. Funct. Mater.* **26**, 5297 (2016).
 - [39] A. Pisoni, J. Jacimovic, O. S. Barisic, M. Spina, R. Gaál, L. Forró, and E. Horváth, *The journal of physical chemistry letters* **5**, 2488 (2014).
 - [40] A. Kovalsky, L. Wang, G. T. Marek, C. Burda, and J. S. Dyck, *The Journal of Physical Chemistry C* **121**, 3228 (2017).

SUPPLEMENTAL MATERIAL

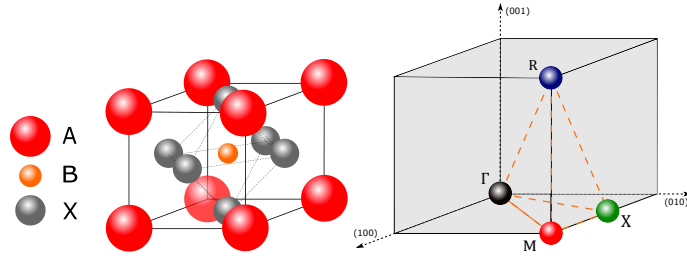


FIG. 1. (a) Schematic representation of the typical ABX_3 perovskite structure. (b) Reciprocal space coordinates for the cubic structure, with high symmetry points highlighted.

Sample Preparation

Methylammonium Lead Bromide: $MAPbBr_3$ single crystals were grown by ITC [1]. A solution of $MAPbBr_3$ was prepared in DMF with 1 M concentration and was filtered with a $0.2 \mu m$ pore size PTFE filters. 3 ml of the obtained solution were then placed into a 5 ml beaker which was introduced in an oven at $80^\circ C$ and kept for 3 h. To increase their size, the formed crystals were extracted from the first beaker and place into another beaker containing fresh filtered solution at the same temperature overnight.

Methylammonium Lead Iodide: $MAPbI_3$ single crystals were grown by ITC [1]. 2 ml of 1 M solution of $MAPbI_3$ in GBL was placed in an oil bath at $80^\circ C$. Then temperature was gradually increased to $110^\circ C$ and kept for 3 h. The formed crystals of ~ 3 mm size were used as seeds for further growth by placing and keeping them in fresh 10 ml 1 M solution at $100^\circ C$ for overnight.

Formamidinium Lead Bromide: $FAPbBr_3$ single crystals were grown by ITC [2]. After the filtration using PTFE filters with a $0.2 \mu m$ pore size, 3 ml of 1 M solution of $FAPbBr_3$ in DMF:GBL (1:1 v/v) were placed into a 5 ml beaker which was introduced in an oven at $40^\circ C$. The temperature was then gradually increased to $52^\circ C$ and kept for 5 h and at $60^\circ C$ for 3 h. The size of the crystal can be further increased through the gradual increase of temperature.

Formamidinium lead Iodide: $FAPbI_3$ single crystals were grown by ITC [2]. A mixture of FAI (0.275 g, 1.6 mmol) and PbI_2 (0.738 g, 1.6 mmol) was dissolved in 2 ml GBL and filtered through a $0.22 \mu m$ PTFE filter. 500 μL of the filtrate was transferred into a 4 ml vial, and placed on a hot plate at $80^\circ C$. The temperature was then gradually increased to $115^\circ C$ and kept for 3 h. The formed crystals of ~ 3 mm size were used as seeds for further growth by placing and keeping them in fresh 1 M solution at 100 - $105^\circ C$ for overnight.

Note: Inelastic neutron scattering measurements on $FAPbI_3$ were particularly challenging since the α -phase, exhibiting photovoltaic properties, is metastable. After a few days, the sample evolves into the yellow phase (δ -phase) that presents no particular physical interest. In principle, the α -phase can be restored for a short period of time (up to 7 days) upon heating, which was indeed demonstrated in small single crystals [2]. However, on large single crystals (as in this particular case) only part of the sample is restored to a single grain and most of the sample remains as a powder. Aligning on a single grain (about 10% of the total volume) was necessary but, nevertheless, we were able to measure dispersing acoustic phonons in that system by performing constant energy scans up to 1.2 meV.

Inelastic Neutron Scattering

The coherent inelastic neutron scattering (INS) spectroscopy was conducted using the triple-axis spectrometers 4F1 and 4F2 located on a cold-neutron source at the reactor Orphée (Laboratoire Léon Brillouin, CEA Saclay), with a fixed neutron wave vector $k_f = 1.55 \text{ \AA}^{-1}$ and a beryllium (Be) filter to remove high-order neutrons from the beam. For the particular case of α - $FAPbI_3$, INS measurements were performed at the IN12 spectrometer from the Institut Laue-Langevin (Grenoble). The conditions were the same, with the exception of the measurements made at the (220)

Bragg reflection, for which the neutron wave vector was changed to $k_f = 1.70 \text{ \AA}^{-1}$ and the Be filter was removed. For all experiments on IN12, a velocity selector was used to remove neutrons with high order harmonics from the incident beam [3]. All samples have been studied in their cubic phase, corresponding to room temperature (RT), except for MAPbI_3 which has been warmed up to 340 K, above its tetragonal-cubic phase transition. Samples were mounted in a scattering plane such that the high symmetry reciprocal directions [100] and [011] were within the horizontal plane. Throughout the present manuscript, the indices refer to the high temperature cubic phase of the HOP lattice. It should be stressed that MA and FA molecules were not deuterated giving rise to a large incoherent neutron scattering from the various hydrogen atoms.

Brillouin light scattering

Brillouin light scattering spectroscopy experiments have also been used to study the angular dispersion of acoustic phonons in MAPbBr_3 and FAPbBr_3 (measurements in the iodide-based samples were not possible with the current set-up as they are not transparent to the laser light). Spectra were recorded at 647.1 nm by using a krypton ion laser and a tandem of Fabry-Perot interferometers where each interferometer is triple passed giving a contrast larger than 10^{-12} .

Experimental Fitting

As in past neutron scattering studies [4], the experimental spectra have been described by the sum of two terms: a damped harmonic oscillator (DHO) corresponding to the probed phonon mode and the above mentioned background signal. In constant \mathbf{Q} -scans, this background is the sum of a quasi-elastic peak (QE) centered at zero energy and a constant. The phonon scattering can be described by the following damped harmonic oscillator (DHO) model

$$S(\mathbf{Q}, \omega) = \left[1 - \exp\left(-\frac{\hbar\omega}{k_b T}\right) \right]^{-1} |F(\mathbf{Q})|^2 \frac{\gamma\omega}{[(\omega^2 - \omega_0^2)^2 + (\gamma\omega)^2]} \quad (1)$$

where ω_0 represents the phonon energy, γ its damping and $F(\mathbf{Q})$ its dynamical structure factor. The prefactor is the phonon population factor. This expression is convoluted by the spectrometer resolution function and used to fit the experimental data. For acoustic phonons, the dynamical structure factor can be written $F(\mathbf{Q}) = \mathbf{Q} \cdot \epsilon$ where ϵ represents the phonon polarization. The wave-vector $\mathbf{Q} = \tau + \mathbf{q}$, where τ is the nearest Bragg spot and \mathbf{q} is the acoustic phonon propagation wavevector. For instance, branches measured around $\tau = (2, 0, 0)$ (as in Fig. 1) are polarized along [100] whatever the propagation vector q is. The sound velocity is derived as $V = \hbar\omega_0/q$.

In all cases, the full scattering function is then convoluted by the 4D spectrometer resolution function as explained in [4]. Some constraints were imposed during the refinements of the data in order to avoid correlations between parameters. In particular, within each dispersing phonon branch group, the dynamical structure factor and the damping γ have been constrained in order to have a consistency within each branch. This way the error bars of the fitted phonon positions are noticeably reduced since the only remaining free parameter is then the phonon energy in constant \mathbf{Q} -scans or its position in momentum in constant energy scans.

Results

TABLE I. Sound velocities of the four different compounds, measured by inelastic neutron scattering (INS) and Brillouin scattering (BS), along various directions. For purposes of comparison, we also present sound velocities obtained by Ultrasonic Scattering (US), from other recent studies [5].

		$V_{TA1} [ms^{-1}] \text{ q} \parallel [110]$	$V_{TA2} [ms^{-1}] \text{ q} \parallel [110]$	$V_{TA} [ms^{-1}] \text{ q} \parallel [111]$	$V_{LA} [ms^{-1}] \text{ q} \parallel [100]$	$V_{LA} [ms^{-1}] \text{ q} \parallel [110]$
α -FAPbI ₃	INS	800±50			1650±150	1150±30
MAPbI ₃	INS	1330±30		1200±50	2300±70	
	US				~3650 ¹	
FAPbBr ₃	INS	900±20	1400±100	1300±20	2700±80	
	BS	620±20	1700±20		2870±30	
MAPbBr ₃	INS	1030±30		1320±20	3000±50	
	BS	955±15	1742±20		2910±10	
	US				~3400 ²	

¹ at 330 K.

² at room temperature (RT).

TABLE II. Mass density and Young elastic modulus along the [100] direction, $E_{[100]}$, of the four perovskite systems in their cubic phases. The Young modulus can be computed from $E_{[100]} = C_{11} - 2C_{12}^2/(C_{11} + C_{12})$. A comparison with the Young modulus determined in two nanoindentation (NI) studies from Rakita *et al.*^a [6] and Elbaz *et al.*^b [7] is presented.

HOP system	Mass Density	Young Modulus		
		INS	BLS	NI
MAPbBr ₃	3880	21.5±0.7	28.2±0.1	17.8±1.12 ^a 19.6±0.3 ^b
FAPbBr ₃	3793	20.9±0.7	26.8±0.7	10.2±0.43 ^a
MAPbI ₃	4117	14.1±1.7		12.0±0.33 ^{a1} 14.3±1.7 ^{b1}
α -FAPbI ₃	4087	9.7±8.2		

¹ Tetragonal phase.

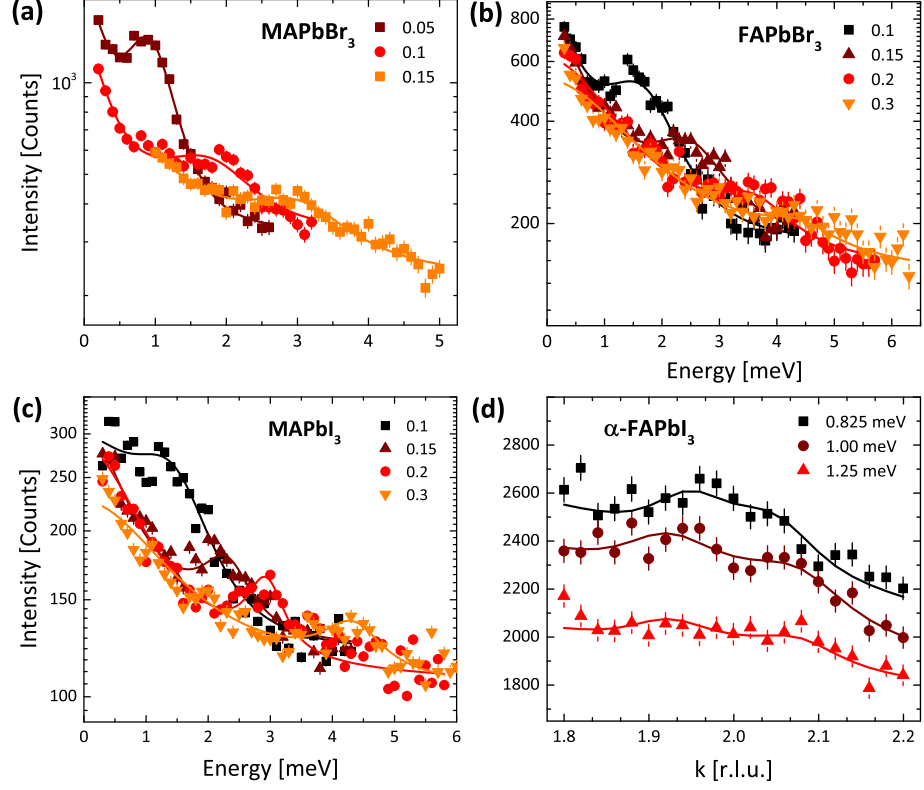


FIG. 2. Longitudinal acoustic phonon spectra measured by inelastic neutron scattering in the cubic phase of (a) MAPbBr₃ (RT), (b) FAPbBr₃ (RT), (c) MAPbI₃ (340 K) and α-FAPbI₃ (RT), for different Q positions going away from the (002) Bragg peak (i.e. $Q = (0\ 0\ 2+k)$) or different energy values.

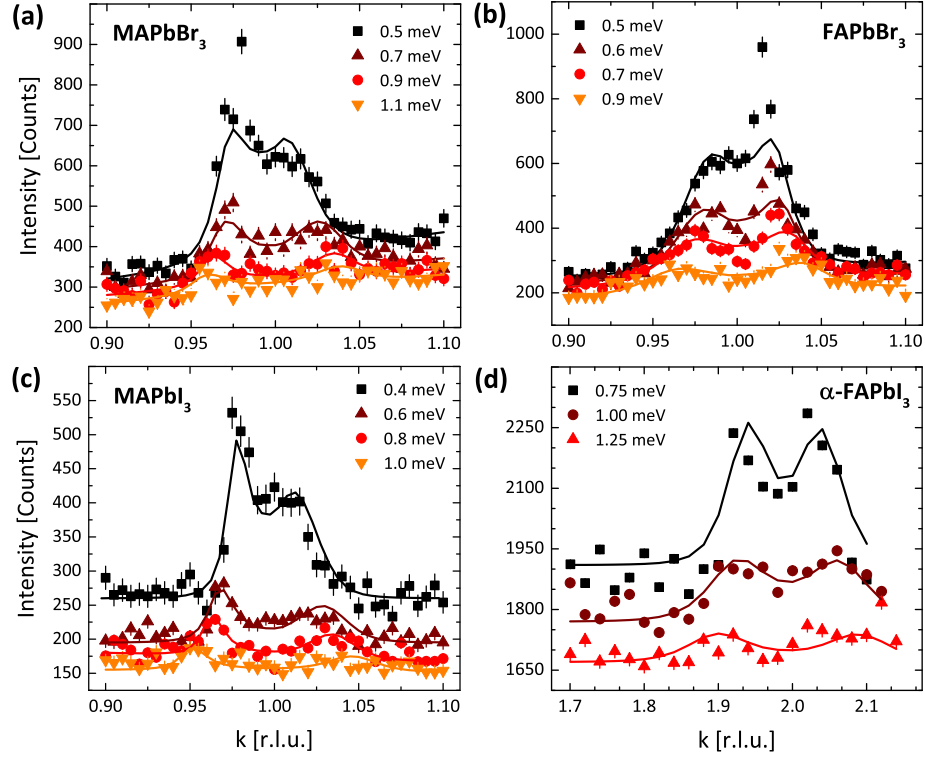


FIG. 3. Transverse acoustic phonon spectra measured by inelastic neutron scattering in the cubic phase of (a) MAPbBr₃ (RT), (b) FAPbBr₃ (RT) and (c) MAPbI₃ (340 K), for different Energy values around the (111) Bragg peak. (d) LA acoustic phonon INS spectra for different Energy values at the (220) Bragg reflection.

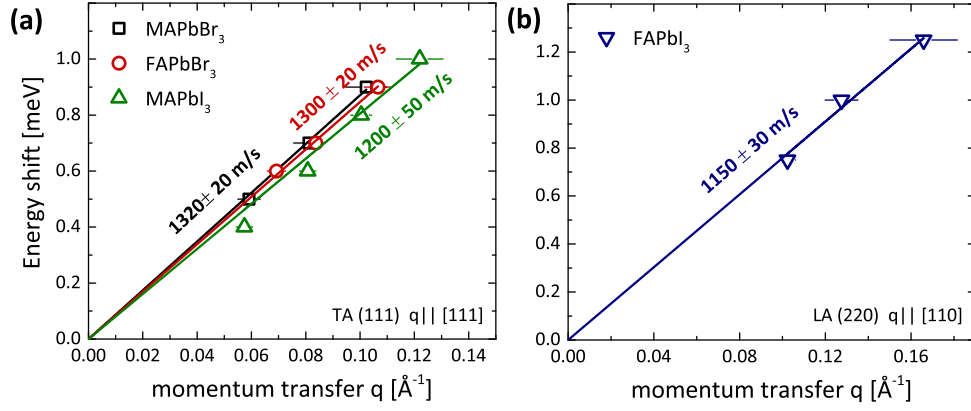


FIG. 4. Acoustic phonon dispersion curves of MAPbBr₃ (RT), FAPbBr₃ and MAPbI₃ (a) TA phonons at the (111) Bragg reflection and (b) α-FAPbI₃ LA phonons near the (220) position. The data for a given configuration (q direction) is regrouped for the different HOP systems and differentiated by different colors and symbols.

REFERENCES

- [1] M. I. Saidaminov, A. L. Abdelhady, B. Murali, E. Alarousu, V. M. Burlakov, W. Peng, I. Dursun, L. Wang, Y. He, G. Maculan, *et al.*, *Nature communications* **6**, 7586 (2015).
- [2] A. A. Zhumekenov, M. I. Saidaminov, M. A. Haque, E. Alarousu, S. P. Sarmah, B. Murali, I. Dursun, X.-H. Miao, A. L. Abdelhady, T. Wu, *et al.*, *ACS Energy Letters* **1**, 32 (2016).
- [3] K. Schmalzl, W. Schmidt, S. Raymond, H. Feilbach, C. Mounier, B. Vettard, and T. Bruckel, *Nuclear Instruments and Methods in Physics Research A* **819**, 89 (2016).
- [4] P. Bourges, M. H. Leme-Cailleau, P. Launois, C. Ecolivet, H. Cailleau, F. Moussa, and A. Mierzejewski, *Physical Review B* **54**, 15002 (1996).
- [5] I. Anusca, S. Balčiūnas, P. Gemeiner, Š. Svirskas, M. Sanlialp, G. Lackner, C. Fettkenhauer, J. Belovickis, V. Samulionis, M. Ivanov, *et al.*, *Advanced Energy Materials* (2017).
- [6] Y. Rakita, S. R. Cohen, N. K. Kedem, G. Hodes, and D. Cahen, *MRS Communications* **5**, 623 (2015).
- [7] G. A. Elbaz, W.-L. Ong, E. A. Doud, P. Kim, D. W. Paley, X. Roy, and J. A. Malen, *Nano Letters* (2017).